Origin of the West Taiwan basin by orogenic loading and flexure of a rifted continental margin

A. T. Lin[1] and A. B. Watts

Department of Earth Sciences, University of Oxford, Oxford, UK

[1] Seismic and well data suggest that the West Taiwan basin developed by orogenic loading and flexure of a rift-type continental margin. The most likely source of the loading is Taiwan, where oblique convergence between the Eurasian and Philippine Sea plates has produced an orogenic belt up to 300 km in length, 100 km in width, and 4 km in height. Flexure modeling shows that surface loading is unable to explain the depth of the West Taiwan basin. Other, subsurface or buried loads are required. Combined surface and buried loading explains the depth and width of the basin. It also accounts for a Bouguer gravity anomaly "high" and flanking "low" over the orogenic belt, a lateral offset of 20–30 km between the peak topography and the maximum depth to the seismic Moho, and evidence for tectonic uplift in the Penghu Islands. The depth of the base of the foreland sequence in the northern part of the West Taiwan basin can be explained well by an elastic plate model with an effective elastic thickness, T_e, of 13 km. While this value is low when compared to most other foreland basins, it is within the range of values derived from rifted continental margins. The northern part of the West Taiwan basin unconformably overlies a passive margin sequence and therefore appears to have inherited the long-term (>1 Myr) flexural properties of the margin. In the southern part of the basin, however, the depth to the base of the foreland sequence dips too steeply to be explained by elastic plate models. This part of the basin therefore appears to be yielding rather than flexing. Differences in the flexural behavior along strike of the West Taiwan foreland basin lithosphere are reflected in seismicity patterns west of the thrust front. The northern part of the basin is associated with a low level of seismic activity, while the south correlates with an abundance of earthquakes, especially at shallow (<25 km) depths. There is a cluster of earthquakes along two extensional faults that were active during rifting of the underlying margin. Therefore lithospheric flexure and fault reactivation may be important contributors to the seismicity of the Taiwan region. *INDEX TERMS:* 1236 Geodesy and Gravity: Rheology of the lithosphere and mantle (8160); 3010 Marine Geology and Geophysics: Gravity; 7230 Seismology: Seismicity and seismotectonics; 8120 Tectonophysics: Dynamics of lithosphere and mantle—general; *KEYWORDS:* gravity anomaly, flexure, foreland basin, seismicity

1. Introduction and Background

[2] Foreland basins are deep depressions of the continental crust that form in compressional plate settings. The depressions are usually flanked by one or more orogenic belts and are infilled by a substantial thickness (up to 10 km) of sediment. The stratigraphic record of foreland basins is a "tape recorder" of the tectonic and erosional history of the flanking orogenic belt and their "architecture" provides information on the physical properties of the underlying lithosphere.

[3] It is generally accepted [e.g., *Price*, 1973; *Beaumont*, 1981; *Jordan*, 1981] that foreland basins develop by flexure of the lithosphere in front of migrating orogenic loads. These include surface as well as buried loads. Surface loads comprise the thrust and fold belts that make up the topography of orogenic belts. Buried loads, on the other hand, include loads that act within and beneath the crust due to overthrusting of one, relatively dense, crustal block over another [e.g., *Holt and Stern*, 1994], subduction of crust and mantle that had already been thinned during a previous extensional event [e.g., *Karner and Watts*, 1983], or a dense downgoing slab [e.g., *Royden*, 1993].

[4] The relative importance of surface and buried loads varies within and between different orogenic belts. Foreland basins that flank some orogenic belts (e.g., Himalaya [*Karner and Watts*, 1983; *Lyon-Caen and Molnar*, 1983], Papua-New

---

[1]Now at Department of Earth Sciences, National Central University, Jungli, Taiwan.
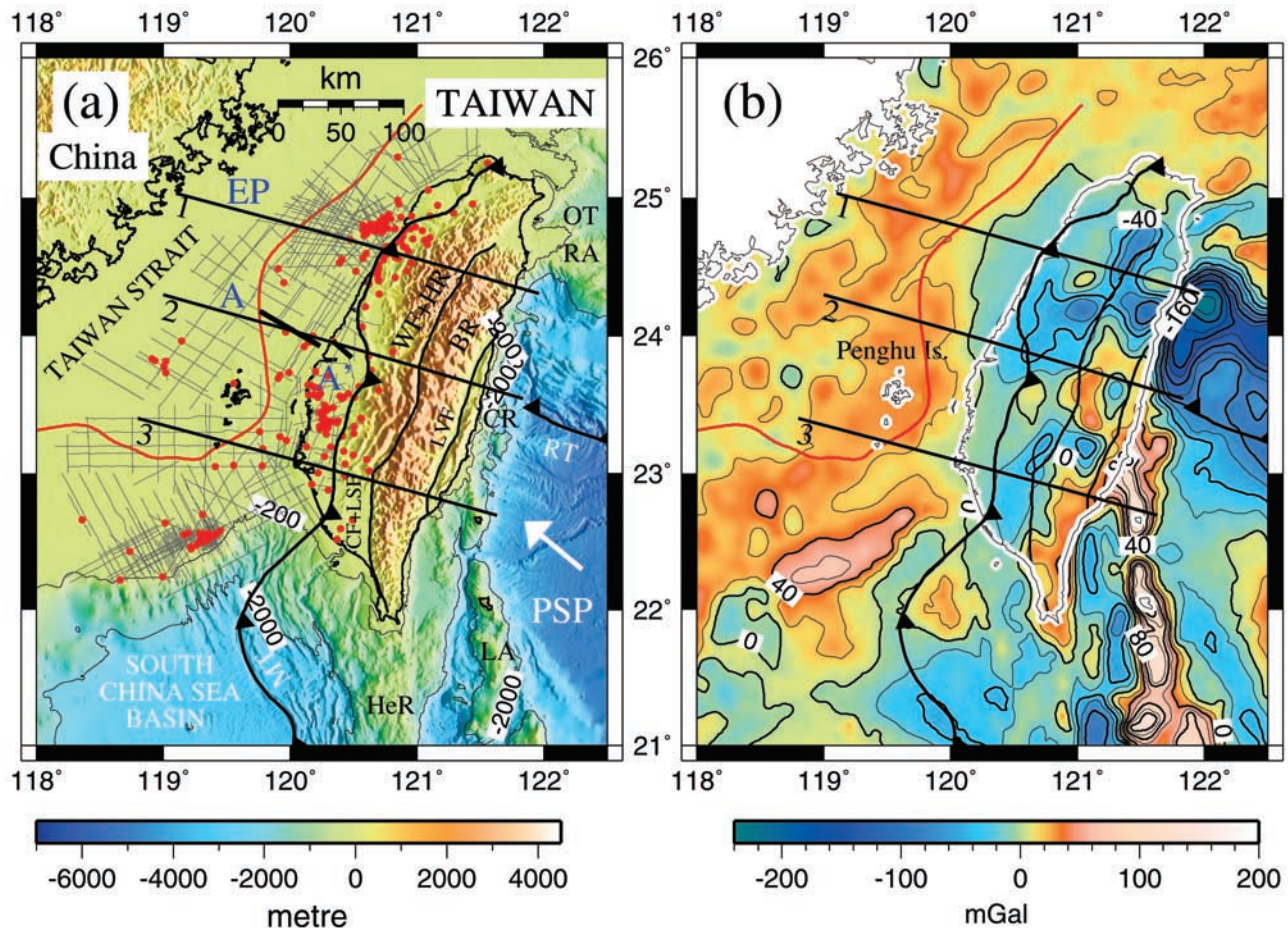
Figure 1. Topography, bathymetry, and gravity anomalies of the Taiwan region. (a) Topography and bathymetry based on the work by *Liu et al.* [1998]. The thin gray lines and red circles indicate the location of the seismic reflection profile and borehole data used to define the stratigraphy of the Taiwan foreland basin and underlying South China Sea margin. The barbed line indicates the thrust front. Thick red line indicates the westernmost edge of the Taiwan foreland. (b) Gravity anomalies (free-air offshore, Bouguer onshore) based on work by *Hsu et al.* [1998, and references therein]. The Taiwan foreland basin correlates with a gravity anomaly "low" and a flanking "high". The topography, bathymetry, flexure, and gravity anomaly along profiles 1, 2, and 3 are shown in Figures 6, 9, and 10. EP, Eurasian plate; BR, Backbone Range, CF, Chaochou Fault; CR, Coastal Range; HeR, Hengchun Ridge; HR, Hsuehshan Range; LA, Luzon Arc; LSF, Lishan Fault; LVF, Longitudinal Valley Fault; MT, Manila Trench; OT, Okinawa Trough; PSP, Philippine Sea plate; RA, Ryukyu Arc; RT, Ryukyu Trench; WF, Western Foothills.

Guinea [*Abers and Lyon-Caen*, 1990; *Haddad and Watts*, 1999], western Tien Shan [*Burov et al.*, 1990], Zagros [*Snyder and Barazangi*, 1986], and central Andes [*Watts et al.*, 1995]) can be explained mainly by surface loading. Others (e.g., Appalachians [*Karner and Watts*, 1983], Carpathians [*Royden and Karner*, 1984], Urals [*Kruse and McNutt*, 1988], and the Karakorum [*Caporali*, 1995]), however, require buried, in addition to, surface loads.

[5]   One parameter that is sensitive to the type of loading is the Bouguer gravity anomaly [e.g., *Karner and Watts*, 1983]. Surface loading implies a Bouguer anomaly "low" that extends from over the foreland to the orogenic belt. Buried loading is also associated with a low, but over the orogenic belt the low is usually replaced, either wholly or partly, by a high. By comparing the predicted anomalies on the basis of combined surface and buried loading to observations, it has been possible to use the Bouguer anomaly to determine the

relative role of surface and buried loading and the effective elastic thickness, T_e, of the lithosphere that underlies a particular foreland basin. Values vary widely. Some forelands (e.g., Apennines, Dinarides) are associated with low values of 5–15 km [e.g., *Royden*, 1993; *Kruse and Royden*, 1994], while others (e.g., Tarim) are associated with intermediate values of 40–55 km [e.g., *Lyon-Caen and Molnar*, 1984]. Finally, some (e.g., Appalachian/Allegheny) have values as high as 50–70 km [e.g., *Stewart and Watts*, 1997].

[6]   The West Taiwan basin formed by flexure in front of migrating thrust and fold loads in the Taiwan orogenic belt [e.g., *Shiao and Teng*, 1991; *Yu and Chou*, 2001; *Chou and Yu*, 2002]. The basin is of geodynamical interest because it is relatively young (<6.5 Ma) and, importantly, has developed on a preexisting rifted continental margin. *Shiao and Teng* [1991] attributed the basin to end loading of a broken elastic plate with $T_e = 18$–22 km. However, they only used
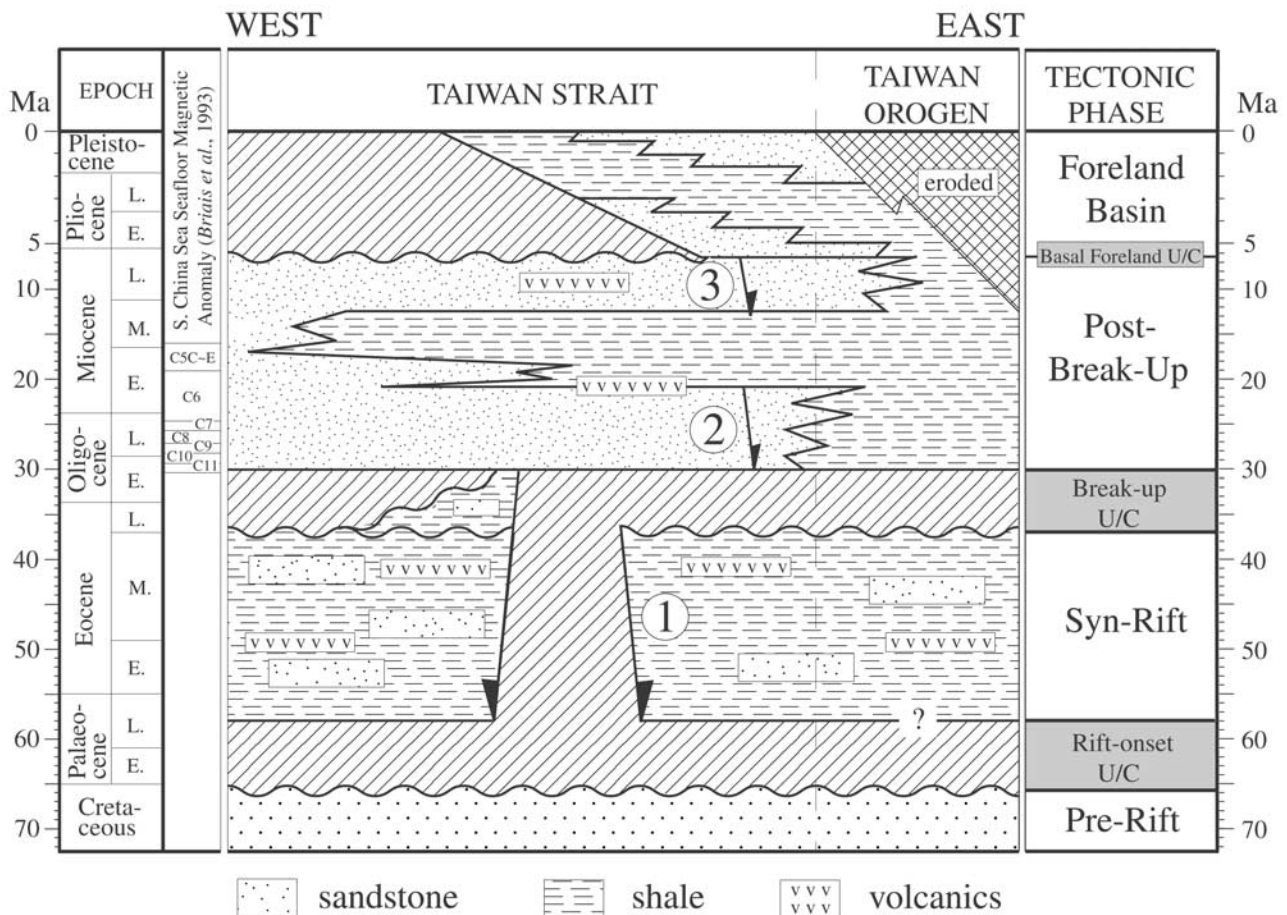
Figure 2. Simplified stratigraphy of the Taiwan region. The synrift and postbreakup sequences formed as a result of rifting of South China Sea during the Paleogene and the formation of oceanic crust in the South China Sea during mid-Oligocene to mid-Miocene [*Briais et al.*, 1993]. The foreland basin sequence formed as a result of the closing of the South China Sea and orogeny in Taiwan about 6.5 Ma. Circled 1, 2, and 3 refer to individual rifting events recognized by *Lin* [2001]. The first rifting event involved the entire margin, while the second and third events were limited to the outer part of the South China Sea margin where the Yichu and B Faults (Figure 11) acted as the main rift basin border faults. U/C, unconformity.

a schematic representation of the base of the foreland basin sequence, attributing it to the top of the Miocene. *Yu and Chou* [2001] and *Chou and Yu* [2002] used seismic and well data acquired by the Chinese Petroleum Corporation of Taiwan to better define the depth to the base of the foreland sequence, but they did not model the flexure.

[7] The purpose of this paper is to use new seismic and well data to estimate the relative role of surface and buried loading and hence the long-term (>1 Myr) thermal and mechanical properties of the lithosphere beneath the West Taiwan basin. The implications of these properties are then examined for (1) the long-term strength of foreland basin lithosphere, (2) the inheritance of rifted margin thermal and mechanical properties during orogeny, and (3) the relationship between flexure, inelastic yielding, and seismicity.

2. Geological and Geophysical Setting

[8] The island of Taiwan comprises a 330-km-long, 100-km-wide, orogenic belt that reaches a maximum height of 4 km (Figure 1a). Dominating the belt is the Backbone Range, which is made up of a central pre-Tertiary metamorphic basement core overlain by Eocene-Miocene metasediments [e.g., *Ho*, 1986]. The Backbone Range is flanked to the east by the Coastal Range and to the west by the Western Foothills and Hsuehshan Range. The Coastal Range is an accreted arc terrain of Miocene to Pleistocene age. The Western Foothills and Hsuehshan Range, on the other hand, are a thrust and fold belt that is made up of Eocene-Pleistocene clastic sediments.

[9] As *Teng* [1990] and others have pointed out, Taiwan is the consequence of the oblique collision between the Eurasian (EP) and Philippine Sea (PSP) plates (e.g., Figure 1a). This convergent plate boundary links opposite verging subduction zones [*Kao et al.*, 1998, 2000]. To the east, the Philippine Sea plate is being subducted beneath the Eurasian plate at the Ryukyu Trench. To the south, oceanic crust of the South China Sea is being subducted beneath the Philippine Sea plate at the Manila Trench. In Taiwan the collision has resulted in the accretion of a number of tectonically distinct
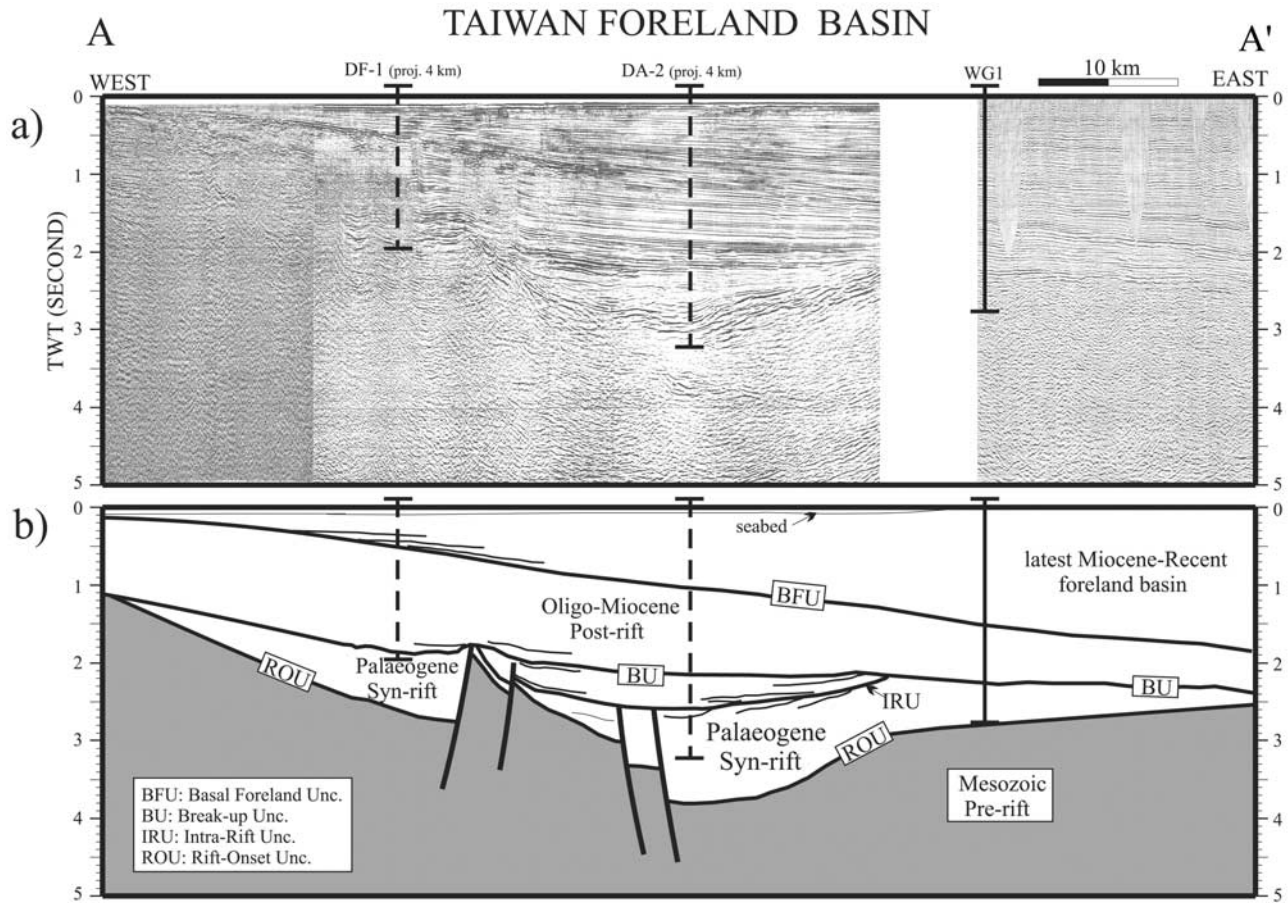
Figure 3. Seismic reflection profile AA′ (Figure 1a) showing the flexure of the synrift and postrift sequences of the South China Sea margin by the Taiwan foreland basin. The base of the foreland basin is defined by an unconformity (BFU) which is unfaulted and separates onlapping foreland basin sequences above from margin-related synrift and postrift sequences below. The thick solid and dashed lines show the location of three deep wells that are located within 4 km of the profile. TWT, two-way travel time. (a) Original profile. (b) Line drawing.

island arc terrains. *Hsu and Sibuet* [1995] suggested that the collision involved the Luzon Arc and extension of the Ryukyu island arc and back arc system. However, a majority of workers [e.g., *Suppe*, 1981] consider a model in which Taiwan resulted from the collision of the Luzon Arc with the Eurasian margin of the South China Sea.

[10] Seismic reflection profile and well data show that the South China Sea margin comprises a synrift sequence of late Paleocene to mid-Oligocene age which is overlain by a postrift sequence of late Oligocene to Miocene age (Figures 2 and 3). Open marine (i.e., shelf) and nonmarine sediments with some intercalated basaltic tuffs and lavas characterize the synrift sequence. The postbreakup sequence comprises of alluvial plain to shallow water shelf sediments. There is evidence from backstripping of biostratigraphic data from deep wells in the basin for two subsequent, postbreakup rifting events during the Oligocene and Miocene [*Lin*, 2001].

[11] The West Taiwan foreland basin unconformably overlies the South China Sea rifted margin. In the north the basin trends across the Taiwan Strait, at an angle to the underlying Nanjihtao and Taihsi-Taichung synrift basins (NJB and TTB in Figure 4). In the south, the basin swings to the west and follows more closely the trend of the underlying Tainan basin (TNB), a postbreakup rift basin. Stratigraphic, lithofacies, and well data suggest that the West Taiwan basin is of latest Miocene to Recent age and comprises a coarsening upward sequence of shallow water clastics and fluvial sediments (Figure 2). Sediments are thickest in the region of the thrust front where they range from 2.5 to 6 km. They thin toward the west, pinching out midway across the Taiwan Strait.

[12] Structural elements of the Taiwan region are reflected in the gravity anomaly field (Figure 1b). The largest-amplitude negative free-air gravity anomalies correlate with the Ryukyu Trench and the largest positive anomalies with the northward extension of the Luzon volcanic arc. The West Taiwan basin is associated with a negative anomaly of up to −60 mGal that is flanked to the west by a broad region of positive anomalies of ∼20 mGal. A free−air "edge effect" anomaly high and flanking low correlate with the South China Sea rifted margin, southwest of Taiwan.

[13] Seismic refraction data show large crustal thickness variations in the region. The crust thins from ∼28−30 km beneath the Taiwan Strait to ∼8 km beneath the South China Sea [*Nissen et al.*, 1995; *Yeh et al.*, 1999] and
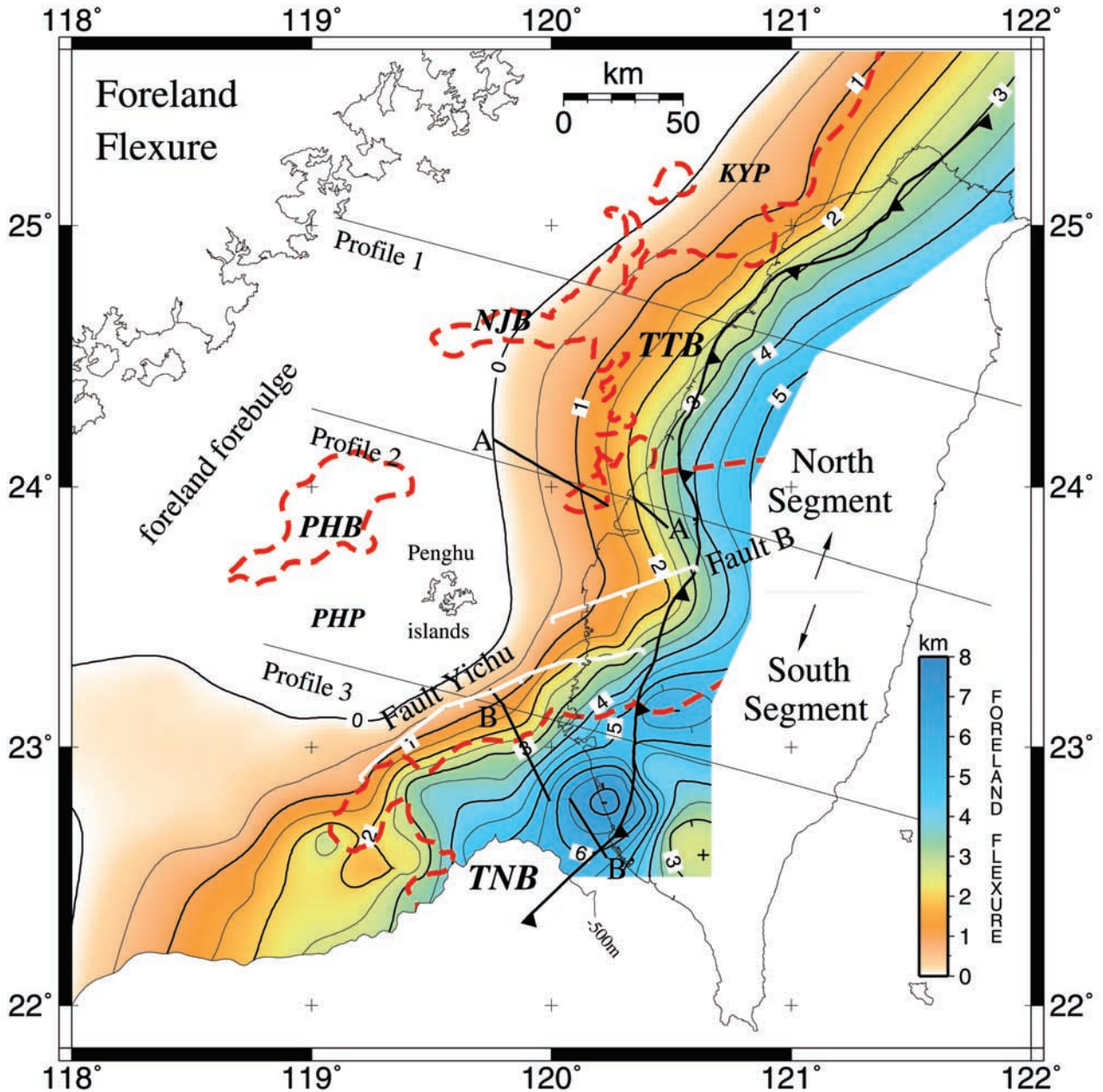
Figure 4. Contour map showing the depth to the base of the foreland sequence in the West Taiwan basin. The dashed lines show the approximate boundary of the synrift basins that developed prior to collision at ~6.5 Ma. Faults Yichu and B are two basin-bounding normal faults that separate the Tainan Basin (TNB) to the south and the Taihsi-Taichung Basin (TTB) to the north. Seismic reflection profiles AA′ and BB′ are shown in Figures 3 and 13, respectively. KYP, Kuanyin Platform; NJB, Nanjihtao Basin; PHB, Penghu Basin; PHP, Penghu Platform.

~10 km beneath the Philippine Sea [*Yang and Wang*, 1998]. The greatest crustal thickness occurs beneath Taiwan where the crust increases from ~30 km beneath the Coastal Plain to 35 km beneath the Western Foothills and Hsuehshan Range to a maximum of 45–50 km beneath the Backbone Range [*Yeh et al.*, 1998].

3. Surface Loading

[14] It is useful when considering the state of isostasy in orogenic belts to consider the topography as a load on the surface of the lithosphere that responds by some form of downwarping. According to the Airy model, for example, topographic highs are underlain by a deep crustal "root" which projects downward into the underlying mantle.

[15] The existence of large-amplitude Airy isostatic anomalies at orogenic belts suggests, however, problems with the model. The Himalaya thrust and fold belt, for example, is associated with positive Airy isostatic anomalies of >+60 mGal, while the flanking Indo-Gangetic foreland basin correlates with negative anomalies of <−100 mGal [*Qureshy*, 1969]. Similar large-amplitude Airy
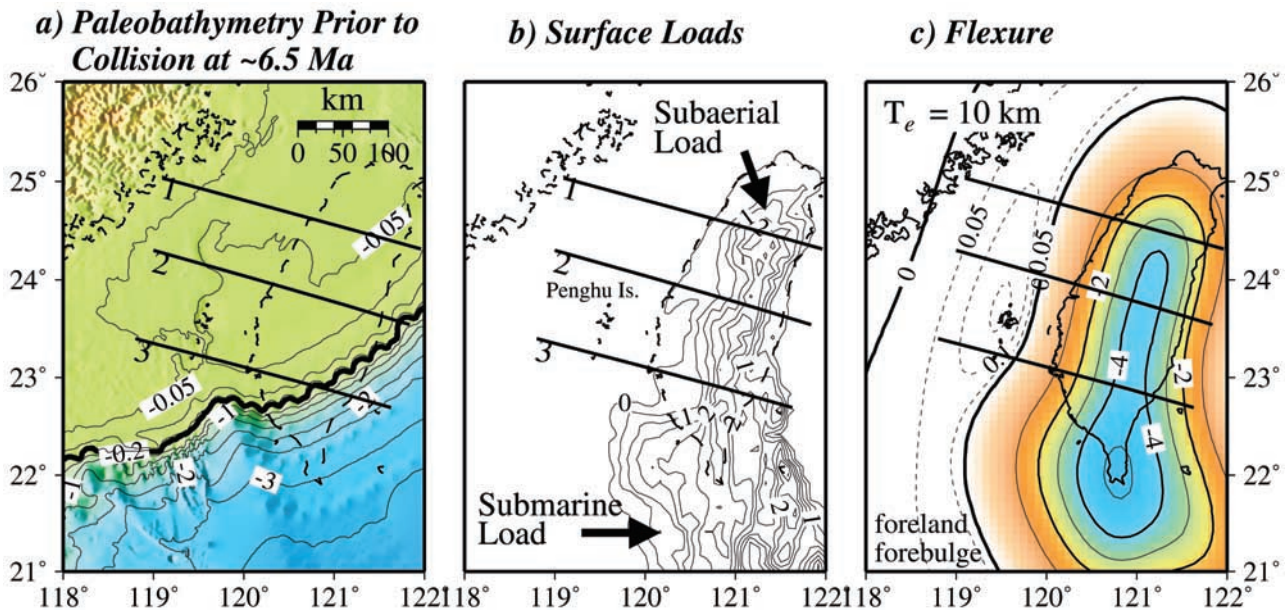
Figure 5. Paleobathymetry, surface loads, and flexure of the South China Sea continental margin. Profiles 1, 2, and 3 are shown in Figure 6. (a) Paleobathymetry of the margin at ∼6.5 Ma based on biostratigraphic and lithofacies data onshore and offshore Taiwan. (b) Surface loads obtained by subtracting a 5 × 5 min grid of the present-day topography and bathymetry of the margin (e.g., Figure 1b) from the paleobathymetry. The surface loads comprise of both a subaerial and submarine component. (c) Flexure due to surface loads on a 3-D elastic plate with T_e = 10 km. Other parameters are as listed in Table 1. The flexure comprises of a depression beneath where the loads are applied and a bulge in flanking regions. Contour intervals in the flexure and bulge regions are 1 km and 50 m, respectively.

isostatic anomalies correlate with the Zagros [*Snyder and Barazangi*, 1986], central Andes [*Watts et al.*, 1995], and Alps [*Heiskanen and Vening-Meinesz*, 1958]. The anomalies indicate that beneath the thrust and fold belt the Moho is shallower than predicted by an Airy model, whereas beneath the foreland basin it is deeper.

[16]   One explanation for the isostatic anomalies is that the crust does not respond to surface loads locally as an Airy model would predict but by flexure over a broad region. *Karner and Watts* [1983], for example, showed that the Bouguer anomaly low over the Lesser and Greater Himalaya and flanking Indo-Gangetic foreland basin could be explained by surface loading of an elastic plate with a break in the region of the Indus-Tsangpo suture and a T_e in the range 80–100 km.

[17]   In Taiwan, convergence between the Eurasian and Philippine Sea plates has resulted in the superposition of a surface topographic load on a rifted continental margin. Topographic and bathymetric maps (e.g., Figure 1a) suggest that this load is made up of both an onshore (i.e., subaerial) and offshore (i.e., submarine) component. The subaerial load represents the exhumed rifted margin and accreted island arc materials that are now exposed in the Taiwan orogenic belt. The submarine load, however, represents the bathymetric "highs" associated with the Hengchun Ridge and the seaward extension of the Luzon Arc.

[18]   We have used a three-dimensional (3-D) flexural response function technique [e.g., *Walcott*, 1976] to quantify the contribution of surface loading to the development of the West Taiwan basin. Figure 5 illustrates our approach. First, biostratigraphic, well and lithofacies data were used to

reconstruct the paleobathymetry of the South China Sea rifted margin prior to collision between the Eurasian and Philippine Sea plates at 6.5 Ma. According to these data, western Taiwan and the Taiwan Strait were in a fluvial to shallow shelf setting prior to collision [e.g., *Ting et al.*, 1991; *Yu*, 1997; *Lin*, 2001]. In contrast, the Hengchun Peninsula, in southern Taiwan, was in a slope setting [e.g., *Sung and Wang*, 1986]. We therefore assume that prior to collision the shelf break was in the vicinity of southern Taiwan and that its strike followed that of the present-day shelf break. The restored bathymetry is shown in Figure 5a. The surface load (Figure 5b) was estimated by subtracting a 5 × 5 min grid of the present-day topography and bathymetry of the Taiwan region from the restored bathymetry.

[19]   Figure 5c shows the flexure that would result from combined subaerial and submarine surface loading. The calculations are based on a continuous elastic plate with T_e = 10 km and assume that sediments infill the flexural depressions up to a horizontal surface. Other parameters assumed in the calculations are listed in Table 1. The load density of 2600 kg m^{-3} is similar to the 2570 kg m^{-3} assumed by *Yen et al.* [1994] for the gravity terrain correction and is probably a representative density of the surface rocks that make up the orogen. The infill density of 2500 kg m^{-3} is based on well log data. It is less than that of the surface load, reflecting the fact that sediments in foreland basins have, in large part, been derived from the loads that cause them and therefore will appear less consolidated and hence less dense than the surface loads.

Table 1. Physical Parameters Used in the Flexural Analyses and Gravity Reductions

Parameter	Definition	Value
ρ_w	water density	1030 kg m^{-3}
ρ_l	topographic load density	2600 kg m^{-3}
ρ_{infill}	basin-infill density	2500 kg m^{-3}
ρ_c	crustal density	2800 kg m^{-3}
$\Delta\rho_b$	buried load density contrast	200 kg m^{-3}
ρ_m	mantle density	3200 kg m^{-3}
tc	crustal thickness at zero topography	28.0 km
g	gravitational acceleration	9.81 m s^{-2}
G	gravitational constant	6.673×10^{-11} m^3 kg^{-1} s^{-2}
E	Young's modulus	1×10^{11} Pa
ν	Poisson's ratio	0.25

[20] As would be expected, the largest flexure (up to 4 km) occurs beneath the main subaerial and submarine load centers. Because of the strength of the plate, however, the flexure extends into regions beyond where the surface loads are applied. The flexural depression, for example, extends 40–80 km west of the Taiwan coastline, just to the east of the Penghu Islands. Beyond the depression, the models predict a flexural bulge which extends from the continental margin, across the Taiwan Strait, intersecting the Chinese mainland in the region of Fujian Province.

[21] A number of similarities exist between the calculated flexural depression and the stratigraphic architecture of the West Taiwan basin, as illustrated in Figure 4. The flexure model successfully predicts the "pinch-out" at the western edge of the basin and its "swing" to the north and south of the Penghu Islands. Moreover, the calculated flexure is greatest in the south where there are both subaerial and submarine surface loads, which is also in accord with observations.

[22] When calculated and observed profiles of the flexure are compared, however, significant discrepancies arise. The main problem is that the calculated flexure is significantly less than the depth to the base of the foreland sequence. This is the case, as Figure 6 shows, irrespective of the T_e that is assumed. Models with a low T_e (e.g., 5 km) predict the depth of the basin. However, the model basin is too narrow compared to the observed. Models with a high T_e (e.g., 20 km) predict the width, but the depth of the basin is too low. Therefore surface loading of a continuous elastic plate is unable to fully explain the shape of the foreland basin inferred from stratigraphic and well data.

[23] One possibility is that rather than being continuous, the plate is broken. A broken plate model has been used in other convergent plate boundary settings (e.g., Appalachian, central Andes, and Himalayas) where it successfully explains the Bouguer gravity anomaly and, in those basins where stratigraphic data are available, the depth of the foreland basin sequence.

[24] Figure 7 compares the predicted flexure based on a 2-D broken plate model to the observations along profile 2 (e.g., Figure 4) of the central West Taiwan basin. We selected a 2-D rather than a 3-D model because it is mathematically simpler. Moreover, profile 2 crosses the central part of the orogen where, as Figure 7a shows, the differences between 2-D and 3-D continuous plate models are small. The predicted flexure has been computed for a $T_e = 13$ km and a plate break located along the trend of the Longitudinal Valley. The Longitudinal Valley is the most likely locality, we believe, for a plate break since it marks
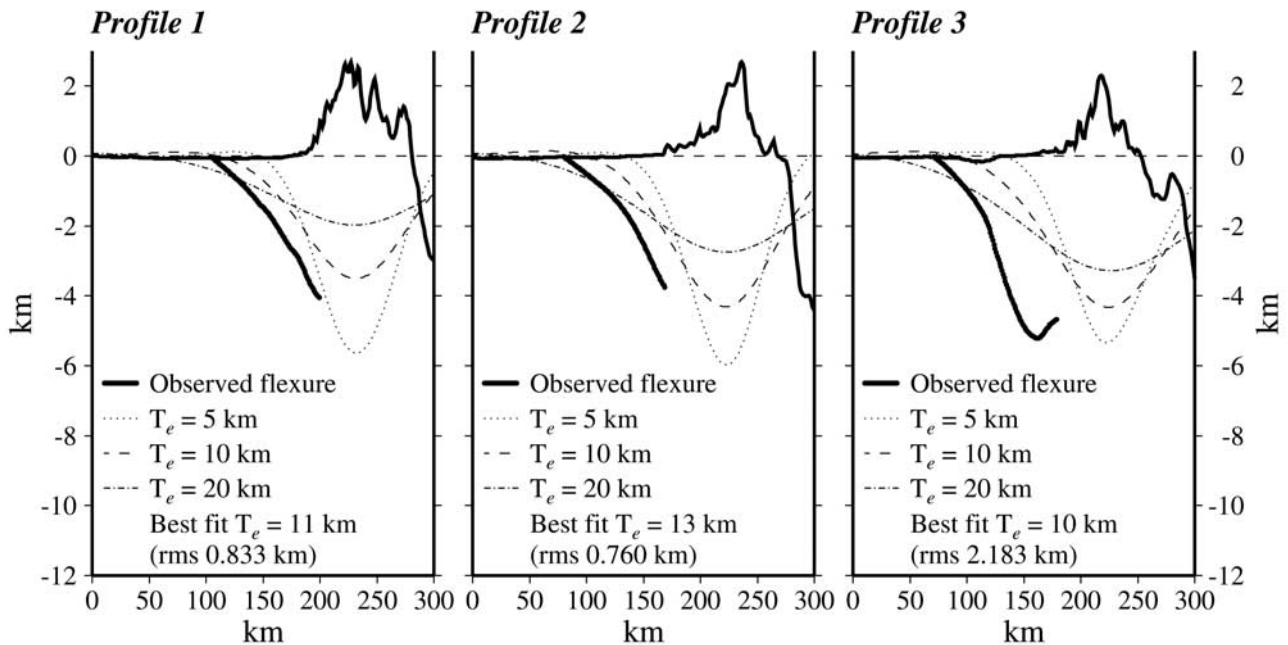
Figure 6. Comparison of the predicted flexure due to surface loading to observations of the depth of the Taiwan foreland basin. The location of profiles 1, 2, and 3 is shown in Figures 1 and 5. The predicted flexure is based on a continuous plate model with $T_e = 5$, 10, and 20 km. The observed depth of the foreland basin is based on the contour map in Figure 4. The best fit to profiles 1, 2, and 3 is for $T_e = 11$, 13, and 10 km and a RMS difference of 0.83, 0.76, and 2.20 km, respectively.

a) Crustal Structure and Flexures along Profile 2

Taiwan foreland basin

A — A'   WF   HR   BR   Coast   CR

Crust

2800 kg m⁻³

Airy Moho

3D continuous
T_e = 13 km
2D broken

Seismic Moho

3200   Mantle

— Observed foreland base
— Seismic refraction Moho with error bars (a)
– – Upper/lower crustal interface from seimic refraction(b)
······ Flexure by surface loads (3D continuous plate, T_e = 13 km)
– – – Flexure by surface loads (2D continuous beam, T_e = 13 km)
– · – Flexure by surface loads (2D broken beam, T_e = 13 km)
– – – Airy Moho

(a) from Yeh et al 1998; 1999 (b) from Yeh et al 1998

Plate suture

b) Gravity Anomaly

Seismic section (Fig. 3)

A — A'   positive

Airy

— Observed gravity anomaly
(Bouguer onshore, free-air offshore)
······ 3D continuous plate (T_e = 13 km)
– – – 2D continuous beam (T_e = 13 km)
– · – 2D broken beam (T_e = 13 km)
– – – Airy

negative

Figure 7. Comparison of the predicted crustal structure and gravity anomalies based on surface loading to observations along profile 2. The thick dashed shaded line shows the location of the plate break. The thick shaded line shows the location of the seismic reflection profile in Figure 3. (a) Crustal structure and flexure. The thick solid line shows the depth of the base of the Taiwan foreland basin based on stratigraphic and well data. The thin solid line shows the depth to the refraction Moho. The thin shaded dashed line shows the upper/lower crust interface based on seismic refraction data. The thin dashed lines show the calculated flexure of the base of the foreland basin sequence (i.e., the surface of the flexed crust) and Moho (i.e., the base of the flexed crust) based on 2-D and 3-D continuous and 2-D broken plate. Also shown is the predicted Moho based on the Airy model. The figure shows that surface loading is unable to explain the depth of the refraction Moho or its lateral offset from the peak topography. (b) Gravity anomaly (free-air offshore, Bouguer onshore). Thick solid line is the observed data. Thin dashed lines show the calculated anomalies based on Airy and the 2-D and 3-D continuous and 2-D broken plate models. The figure shows that surface loading is unable to explain the magnitude of the Bouguer anomaly high over the Backbone Range or the flanking low over the Taiwan foreland basin.

the suture between the Eurasian and Philippine Sea plates. There are significant differences along profile 2 between the predictions of the continuous and broken plate model. The difference is most obvious in the region of the Hsuehshan and Backbone Ranges where continuous plate models predict a smaller flexure than the broken plate model. The difference in the region of the foreland basin is, however, small. Thus, while a broken plate increases the magnitude of the flexure, the increase is limited to the region where the load has been applied.

[25] Our conclusion that surface loading of continuous and broken plates is unable to explain the observed depth to the base of the foreland sequence is in agreement with the available crustal thickness data. Figure 7a compares, for example, the seismic refraction Moho to the calculated Moho assuming surface loading. Figure 7a shows that surface loading of a 2-D continuous and broken plate is unable to explain the depth to the refraction Moho. The discrepancy is largest beneath the Backbone Range where the refraction Moho is laterally offset 20–30 km to the east of, and is up to 15 km deeper than, the Moho predicted by the flexure models.

[26] Finally, surface loading is unable to explain the observed Bouguer gravity anomaly. In particular, the calculated anomaly cannot explain the Bouguer anomaly low over the foreland and the flanking high over the orogen (Figure 7b). The discrepancy is not limited to a single profile. Figure 1b shows that a large-amplitude positive-negative Bouguer anomaly "couple" extends along much of the length of Taiwan. The most likely explanation of the couple, we believe is that other, subsurface or buried, loads are acting on the lithosphere in addition to surface loads.

4. Buried Loading

[27] The possibility that buried loads might be required to explain the depth of foreland basins, in addition to surface loads, has already been suggested at other orogenic belts. The origin of these loads is not always clear, however. They have been variously attributed to overthrusting of one crustal block over another [e.g., *Holt and Stern*, 1994], intrusion of mafic material [e.g., *Tanner and Uffen*, 1960], crust and mantle that had already been thinned by extensional or other processes [e.g., *Karner and Watts*, 1983], or a dense downgoing slab [e.g., *Royden*, 1993]. In those cases where the source is unknown [e.g., *Lyon-Caen and Molnar*, 1984], the buried load has been replaced by a terminal force or bending moment that is applied to the end of the underthrust plate.

[28] Irrespective of its geological interpretation, the Bouguer gravity anomaly high is a useful indicator of the size of the buried load. *Karner and Watts* [1983], for example, used Gauss's theorem to estimate the size of the buried load from terrain corrected gravity measurements over the eastern Alps and Appalachians. They showed that buried loading was an important contributor to the Bouguer gravity anomaly, explaining both the lows over the foreland and the highs over the flanking orogenic belt.

[29] We have used the gravity anomaly to evaluate the role that buried loading may play in the development of the West Taiwan basin. Our procedure involves four main steps. First, the gravity effect of the crustal thickening beneath

Taiwan is calculated assuming an Airy model with a crust and mantle density of 2800 and 3200 kg m^{-3}, respectively, and a zero elevation crustal thickness of 28 km (Figure 8a). Second, the gravity effect of the Airy Moho (the heavy dashed line in Figure 7b) is compared to the observed Bouguer anomaly (solid line). This divides the Bouguer anomaly into a positive part that we attribute to the buried load and a negative part that is the result of flexure due to combined surface and buried loading. Third, the gravity effect of the Airy Moho is subtracted from the observed Bouguer anomaly. Because the bulge area, west of the Taiwan foreland basin, is characterized by a broad positive gravity anomaly which most probably reflects sources at or below the crust, we have added 20 mGal to the calculated Bouguer anomaly of the Airy Moho prior to subtracting it. The resulting Airy isostatic anomaly is illustrated in Figure 8b. Figures 8b and 10a show that the largest (i.e., >+50 mGal) anomalies are limited to the Backbone Range, between the Chaochou and Lishan faults and Longitudinal Valley fault, where they correlate with the outcrop of the pre-Tertiary metamorphic complex, relatively high *P* wave crustal velocities [*Rau and Wu*, 1995; *Lin et al.*, 1998] and, an "upwarp" of the interface that separates the seismic lower and upper crust [*Yeh et al.*, 1998] (Figure 7a).

[30] The next step is to use the positive Airy isostatic anomaly high to determine the equivalent height and hence the size of the buried load for different assumptions about the density contrast between the load and the material that it displaces. We can write, for example, from Green's equivalent layer theorem that

$$t = \frac{\Delta g_c}{2\pi G \Delta \rho_b},$$

where Δg_c is the positive part of the Airy isostatic anomaly, t is equivalent height, $\Delta \rho_b$ is density contrast between the buried load and its surroundings, and G is gravitational constant. A load of height t and density contrast $\Delta \rho_b$ is then placed on the surface of an elastic plate and the flexure calculated for different assumed values of T_e. The calculations in Figure 8c, for example, show the flexure that would result from a 3-D buried load which is denser by 200 kg m^{-3} than the material it displaces and has been emplaced on the surface of an elastic plate with $T_e = 13$ km. The maximum flexure occurs in the center of Taiwan where it correlates with the largest-amplitude Airy isostatic gravity anomaly. The flexure extends beyond the high, however, to beneath the Taiwan Strait because of the flexural strength of the plate.

[31] The final step is to calculate the combined effect of surface and buried loading on the flexure. Figure 8d shows, for example, the flexure for $T_e = 13$ km. The flexure is similar in overall trend to the case of surface loading only (i.e., Figure 5c). The main difference is that the amplitude of the flexure is larger and the basin is slightly wider.

[32] Figure 9 compares the depth to the base of the foreland sequence along profile 2 to the calculated flexure based on combined surface and buried loading. Figure 9 shows that buried loading increases the amplitude of the flexure caused by surface loading by up to 1 km beneath the thrust front. The calculated flexure, however, still does not fully explain the depth of the base of the foreland sequence.
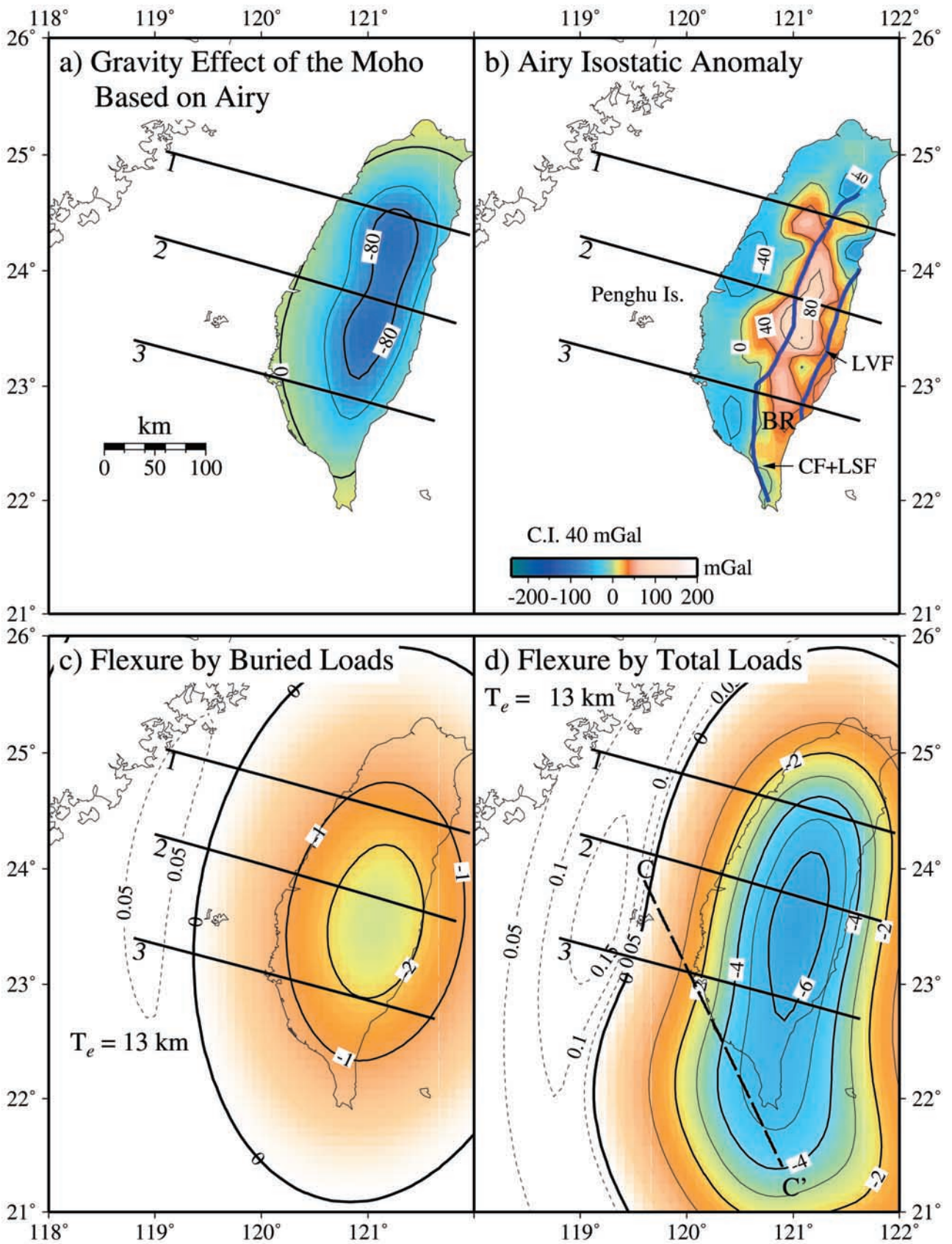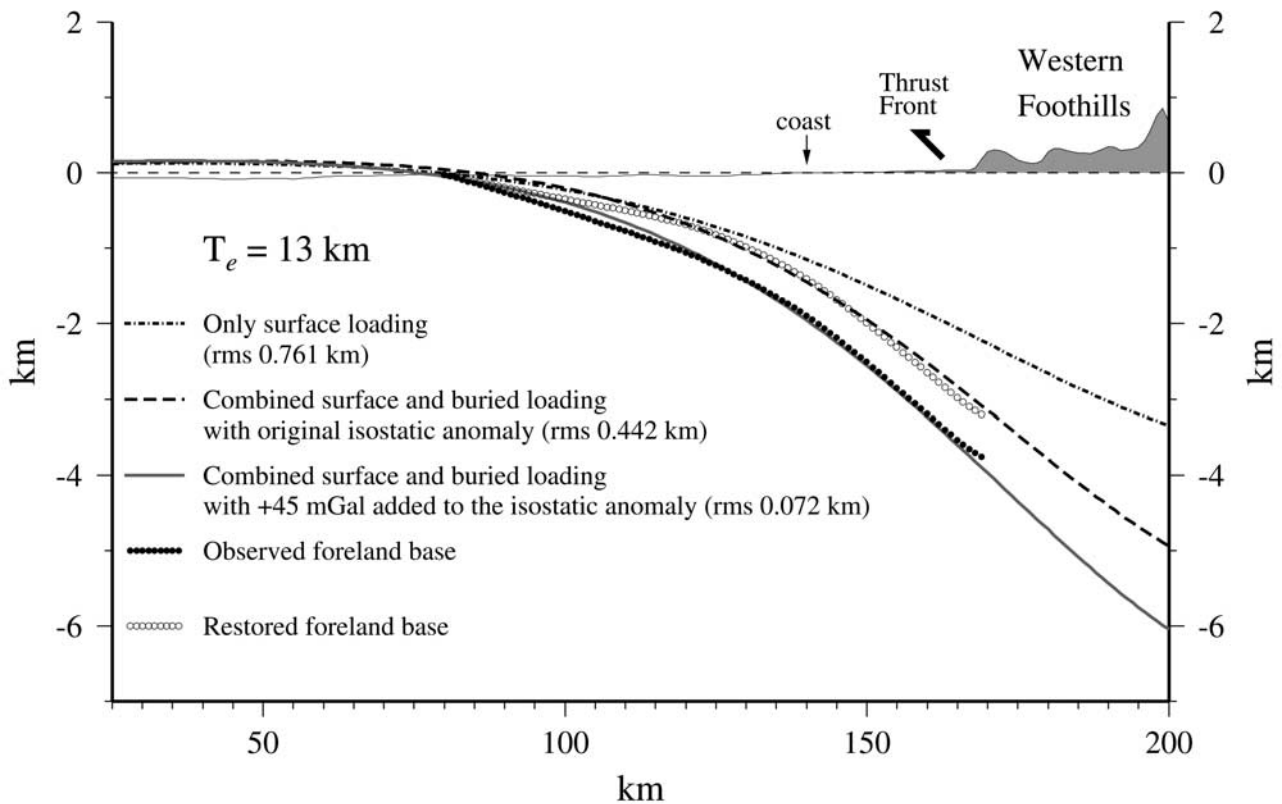
Figure 9. Comparison of the observed depth of the West Taiwan basin to the calculated flexure based on combined surface and buried loading along profile 2. The solid circles show the observed depth of the base of the foreland sequence based on the stratigraphic and well data. The open circles show the depth corrected for the effects of compaction of the underlying rifted margin sediments by the foreland basin sediment fill. The lines show the calculated flexure based on surface and buried loading and $T_e = 13$ km. Dash-dotted line shows the flexure based only on surface loading. Dashed line shows the flexure based on combined surface and buried loading. Solid line shows the flexure based on combined surface and buried loading with an additional load, equivalent to +45 mGal.

[33] There are two possible explanations for the discrepancy. First, we may have underestimated the magnitude of the buried load and hence the flexure. This possibility arises if the Airy model fails to provide an adequate description of the crustal thickening beneath the orogenic belt. That this might be the case is illustrated in Figure 7. Figure 7 shows that the refraction Moho is significantly deeper than the Airy Moho and hence the Moho computed assuming flexure. A deeper Moho would yield a more negative Bouguer anomaly due to crustal thickening and hence more positive isostatic anomalies, a larger buried load, and greater flexure. Second, even if we accept that the Airy model adequately describes the crustal thickening, there is still a significant high remaining after it is subtracted from the observed anomaly. The high due to the buried load begins, for example, at the inflection points in the observed Bouguer anomaly and not as we have assumed at the "crossover" point between the anomaly and the gravity effect of the crustal thickening based on the Airy model.

[34] Figure 9 shows that an increase in the buried load by the equivalent of +45 mGal is all that is needed in order to bring the observed and calculated flexure into agreement. The calculated flexure which best fits the observed (in a least squares sense) is based on $T_e = 13$ km.

[35] Another possibility is that the buried loads based on the departures from Airy isostasy are correct and it is the

Figure 8. (opposite) Gravity anomalies and the role of buried loading in the Taiwan region. (a) The calculated gravity effect of the Moho assuming an Airy model of isostatic compensation. (b) The Airy isostatic anomaly obtained by subtracting the calculated gravity effect of the Moho based on Airy from the observed Bouguer gravity anomaly. The Backbone Range (BR) is associated with a belt of positive Airy isostatic anomalies which we interpret as the result of buried loading within the crust. (c) The calculated flexure that results from buried loading. The buried loads were determined by calculating the equivalent load from the positive Airy isostatic anomaly (plus an additional +45 mGal; see text for discussion) for different density contrasts between the load and its surroundings. The flexure was calculated by placing these loads on the surface of a 3-D elastic plate with $T_e = 13$ km. (d) The flexure due to combined surface and buried loading. The bending stress in the uppermost part of the flexed plate along profile CC' is shown in Figure 12.

depth of the foreland basin that is incorrect because of mechanical compaction of the underlying rifted margin. We have assumed in the calculations thus far, for example, that the "basement" that underlies the foreland basin sequence is fully compact. This is unlikely because the synrift and postrift margin sequences that make up basement may experience further compaction once they are reloaded by the sediments which make up the foreland basin. We may therefore need to compare the calculated flexure not to the present depth of the base of the foreland basin sequence which includes a component of subsidence from compaction of the underlying margin but to the depth that it would have been in the absence of compaction. We estimated the amount of this compaction, using porosity versus depth curves [*Lin*, 2001] derived from sonic logs, and find that it is up to 750 m in the region of the thrust front.

[36] Figure 9 shows that when the amount of subsidence due to compaction of the underlying margin is calculated and subtracted from the observed depth of the foreland basin, then an excellent fit is obtained between the observed flexure and the calculated flexure based on an Airy definition of the buried load.

[37] Figure 10 compares the observed flexure and gravity anomaly along all three profiles of the West Taiwan basin to calculations based on surface and buried loading and different values of T_e. Figure 10 shows that the depth of the foreland basin sequence along profiles 1 and 2 are well explained by the flexure model. The corresponding "best fit" T_e values for both these profile is 13 km. Lower values predict too large a flexure and too narrow a basin, while higher values predict too small a flexure and too wide a basin. The gravity effect of the flexure based on T_e = 13 km explains well the decrease in Bouguer anomaly that is observed between the bulge and the thrust front. The discrepancy in the region of the orogenic belt arises because the calculated gravity effect in Figure 10 is based only on the flexure and does not include the effect of the buried load. The depth of the foreland basin sequence and the gravity anomaly along profile 3, however, are not well fit by the flexure models. The best fit between observed and calculated flexure is based on T_e = 16 km, but the calculated flexure cannot explain the steepness of the depth to the base of the foreland basin sequence that is observed on this profile.

5.   Discussion

[38] We have shown in this paper that the West Taiwan basin formed by surface and buried loading of a rifted continental margin. The best fits between observed and calculated flexure were obtained over the northern part of the basin where a T_e value of 13 km has been estimated. The poorest fits were obtained in the southern part of the basin. We now discuss the implications of these results for the T_e structure of the Taiwan foreland lithosphere, the inheritance of geological structures through time, and seismicity patterns in the Taiwan region.

5.1. T_e Structure of the Taiwan Foreland Lithosphere

[39] We estimated T_e along only two profiles of the foreland and so have limited information on spatial changes in the effective elastic thickness of the continental lithosphere that underlies the West Taiwan basin. Profile 1, which crosses the northern part of the basin, is associated with T_e = 13 km. Profile 2 of the central part of the basin requires a similar value. Profile 3, which crosses the southern part of the basin, could not, however, be fit by any of the elastic plate models.

[40] One explanation for these observations is that while the lithosphere beneath the northern part of the basin has been simply flexed, the plate in the south has been loaded to its limit and so has broken rather than flexed. Support for this suggestion comes from the observation that the depth to the base of the foreland sequence is larger (by up to 4 km) along profile 3 than profile 1 or 2. Furthermore, whereas the northern part of the basin trends subparallel to the orogenic belt, at an angle to synrift basins in the underlying rifted margin, the southern part of the basin trends at an angle to the local trend of the orogenic belt, subparallel to the margin.

[41] The T_e determined for the West Taiwan basin is low when compared to other foreland basins such as the eastern Swiss Molasse, Appalachians/Allegheny, and the Chaco Plain (central Andes). However, it is within the range of previous values determined at the Appenines [*Royden and Karner*, 1984], Dinarides [*Kruse and Royden*, 1994], eastern Papua New Guinea [*Abers and Lyon-Caen*, 1990; *Haddad and Watts*, 1999], and the western Swiss Molasse [*Stewart and Watts*, 1997].

[42] Our best fit flexure models predict a bulge to the west of the West Taiwan basin. The bulge crest extends from the present-day shelf break of the South China Sea margin, across a broad bathymetric rise (the Taiwan Bank) that incorporates the Penghu Islands, to the coast of China in the region of Fujian Province. According to the flexure calculations in Figure 5c, which are based on T_e = 10 km, the Penghu Islands are located near the crest of the bulge. However, the calculations in Figure 8d, which are based on T_e = 13 km, show that the Penghu Islands are located close to the node that separates the flexure from the bulge. The Penghu Islands are located between profile 2 where the best fit T_e = 13 km and profile 3 where the plate may have

---

Figure 10.   (opposite) Comparison of the observed flexure and Bouguer gravity anomaly over profiles 1, 2, and 3 of the Taiwan foreland basin to calculations based on combined surface and buried loading. (a) Gravity anomalies. The observed profile (heavy solid line) is based on data in Figure 1b. The calculated gravity anomaly (thick dashed line) are based on the "best fit" T_e values, an additional load equivalent to +45 mGal, and the parameters listed in Table 1. Only the gravity effect of the flexure is shown. (b) Loading ratio obtained by dividing the buried load by the surface load. (c) Foreland basin flexure. The observed profile (heavy solid line) is based on data in Figure 4. The calculated profiles (thin dashed lines) are based on T_e values of 5, 10, and 20 km; an additional load equivalent to +45 mGal; and the parameters listed in Table 1. The thin shaded solid line shows the best fitting profile. (d) Plot of root-mean-square difference between observed and calculated flexure versus T_e, illustrating the resolution of the best fit T_e.
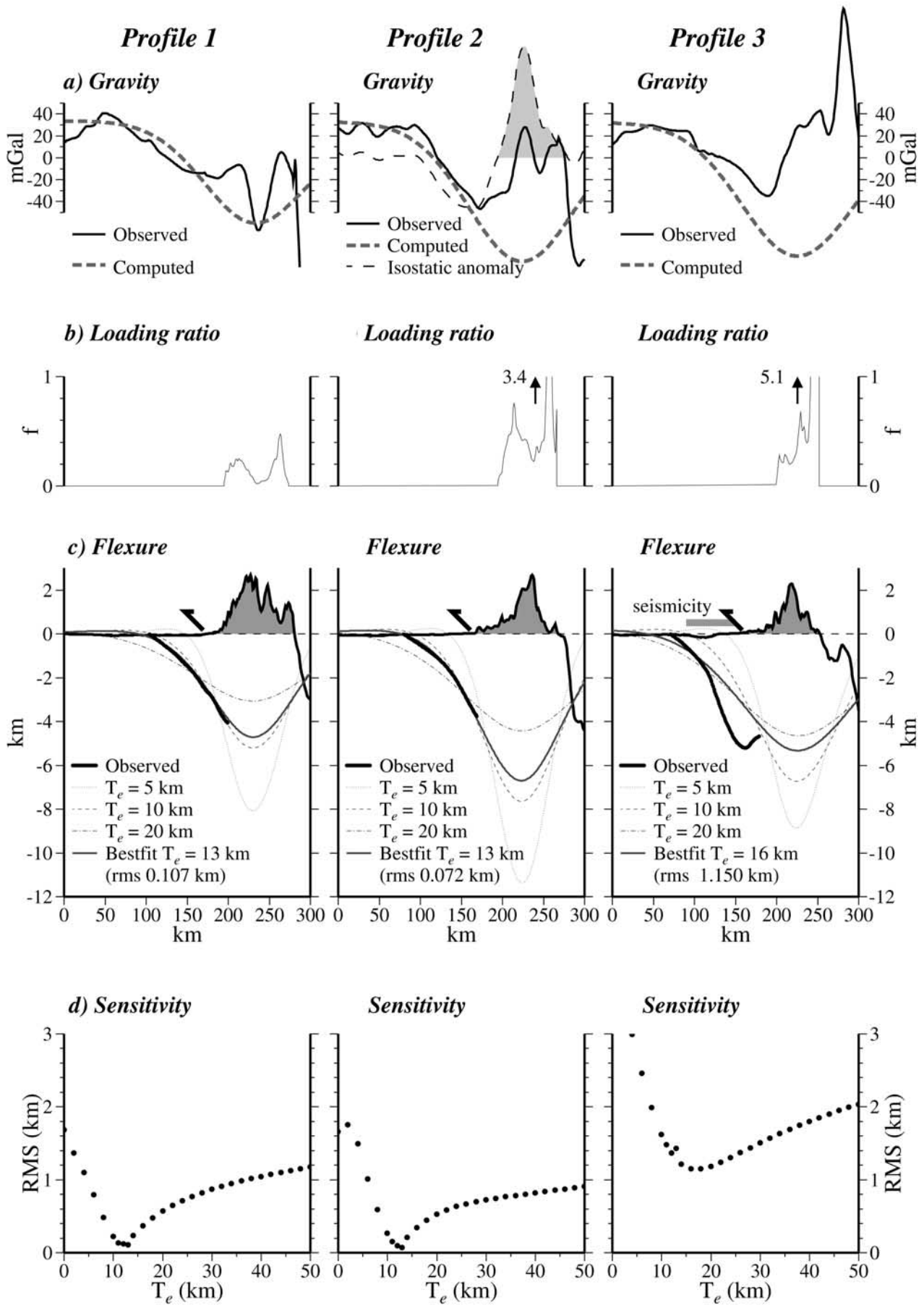
broken rather than flexed. Therefore it is probable that between profiles 2 and 3, $T_e < 13$ km and hence that the Penghu Islands are located within the region of the bulge, as, in fact, is illustrated in Figure 5. It is interesting to note that the Penghu Islands are made up of mid-to late Miocene basalts [*Juang and Chen*, 1992] and so they predate the orogeny in Taiwan. Their uplift may therefore be a consequence of their location on the same bulge that was generated by flexure due to orogenic loading in Taiwan. This interpretation is in accord with the observation of a flat "plane" at levels of 50–60 m and 20–30 m [*Chen*, 1992] above sea level on many of the Penghu Islands. Flexure may not, however, explain all the uplift. There is evidence, for example, on some of the islands of Holocene raised beaches a few meters (<5 m) above sea level which *Chen and Liu* [1996] have attributed to glacial-eustatic sea level changes rather than flexural loading.

5.2. Inheritance and the T_e Structure of Rifted Continental Margins

[43] Probably the most significant feature of the tectonic setting of the West Taiwan basin is its location on the South China Sea continental margin. The T_e structure of the foreland may therefore reflect the long-term (i.e., >1 Myr) thermal and mechanical properties of the underlying rifted margin.

[44] Previous estimates of T_e at rift-type basins in continental margins show a wide range of values. They range, for example, from a low of 5–10 km for the Valencia Trough [*Watts and Torné*, 1992] and Baltimore Canyon Trough [*Watts*, 1988] to a high of 40–60 km for the Salisbury Embayment [*Pazzaglia and Gardner*, 1994], Labrador, and West Greenland margins [*Keen and Dehler*, 1997]. A problem with most of these estimates, however, is that they represent the average response of the lithosphere to sediment loading. They therefore do not refer to a particular crustal type (e.g., stretched continental crust) or age since rifting. At the U.S. East Coast margin, for example, postrift sediments have been deposited over a >300-km-wide region of the margin and have a time duration of 150 Myr. It is therefore difficult using these data to address specific issues such as the T_e structure of stretched crust and whether or not it is able to recover its strength with time.

[45] The advantage of the West Taiwan basin is that it formed by a relatively short-term, discrete, orogenic load that was superimposed on a rifted margin with a reasonably well known rifting history. Profile 1 of the basin, for example, is located above the Taihsi-Taichung Basin, which seismic and well data suggest experienced rifting during ~30–58 Ma [*Lin*, 2001]. Therefore, if the $T_e = 13$ km determined along this profile was acquired at 6.5 Ma (i.e., at the initiation of the collision), then it represents the T_e structure of rifted continental crust ~23.5–51.5 Myr after the rifting event.

[46] The significance of these results is that they support previous suggestions [e.g., *Desegaulx et al.*, 1991; *Watts*, 1992] that when a foreland develops on a rifted margin (due, for example, to closure of an ocean basin), it inherits the T_e structure of the underlying margin. We know from studies of present-day analogues that the T_e structure of rifted margins varies spatially with low values over the stretched part of the margin and higher values over flanking oceanic and continental regions [e.g., *Watts*, 1988]. Whether or not a foreland basin develops on stretched crust depends, however, on a number of factors including the extent to which individual thrust and fold loads are "telescoped" onto the continental interior as a consequence of collision. The low T_e values determined at the Apennines, Dinarides, eastern Papua New Guinea, and the western Swiss Molasse forelands indicate that these basins probably did develop on stretched continental crust. The high T_e forelands, on the other hand, probably reflect their formation on unstretched crust or crust that had not been as stretched during initial rifting. These considerations suggest that tectonic setting, rather than secular cooling history, crustal composition, or strain rate, may be a significant factor in determining the T_e structure of continental lithosphere.

5.3. Seismicity, Curvature, and Yielding

[47] Taiwan is one of the most seismically active regions of the world [e.g., *Wang and Shin*, 1998]. There has been a long history of large (i.e., $M_b > 7$) magnitude earthquakes [*Wu and Rau*, 1998], for example, with the last major one being the Chi-Chi earthquake in 1999 [*Kao and Chen*, 2000].

[48] Figure 11 shows the seismicity of the Taiwan region as derived from local networks during the 8-year period prior to the Chi-Chi earthquake. The orogen to the east of the thrust front is associated with a high level of seismicity. The foreland basin to the west of the thrust front, in contrast, is associated with a much lower level of seismicity. The main exception is in a narrow region of western Taiwan where there is an abundance of relatively shallow (<28 km) earthquakes. The earthquake zone is delineated to the north by Fault B and appears to continue across the thrust front to the western boundary of the Backbone Range.

[49] There is a suggestion in Figure 11 of a relationship between the seismicity pattern in the foreland basin west of the thrust front and the T_e results. The relatively low level of seismicity in the northern part of the basin, for example, is crossed by profiles 1 and 2 where the lithosphere has been gently flexed by the Taiwan orogen. The high level of seismicity in the south, however, is crossed by profile 3 where we could not account for the depth of the base of the foreland sequence using elastic plate flexure models.

[50] In order to examine whether a relationship might exist between flexure and seismicity, we constructed a profile, CC′, that crosses the foreland in the region where the elastic plate model fits poorly and where there is a relatively high level of seismic activity (Figure 12). Figure 12 (bottom) shows all the earthquakes that fall within a 10-km "window" either side of the profile. Figure 12 (top) shows the bending stresses that would have accumulated in the outer part of an elastic plate, which had a similar T_e structure as profiles 1 and 2 of the northern, flexed, part of the basin. The predicted bending stresses are tensile over the foreland basin reaching a maximum of 500 MPa in the region of the coastline. Figure 12 shows a close correlation between the peak bending stress and the high seismicity. This suggests a link between them: the high seismicity is occurring in a region of high tensile bending stresses where it is likely that the plate underlying the foreland would have failed rather than flexed.

[51] There is still the question of why a similar high level of seismicity does not exist along the entire length of the
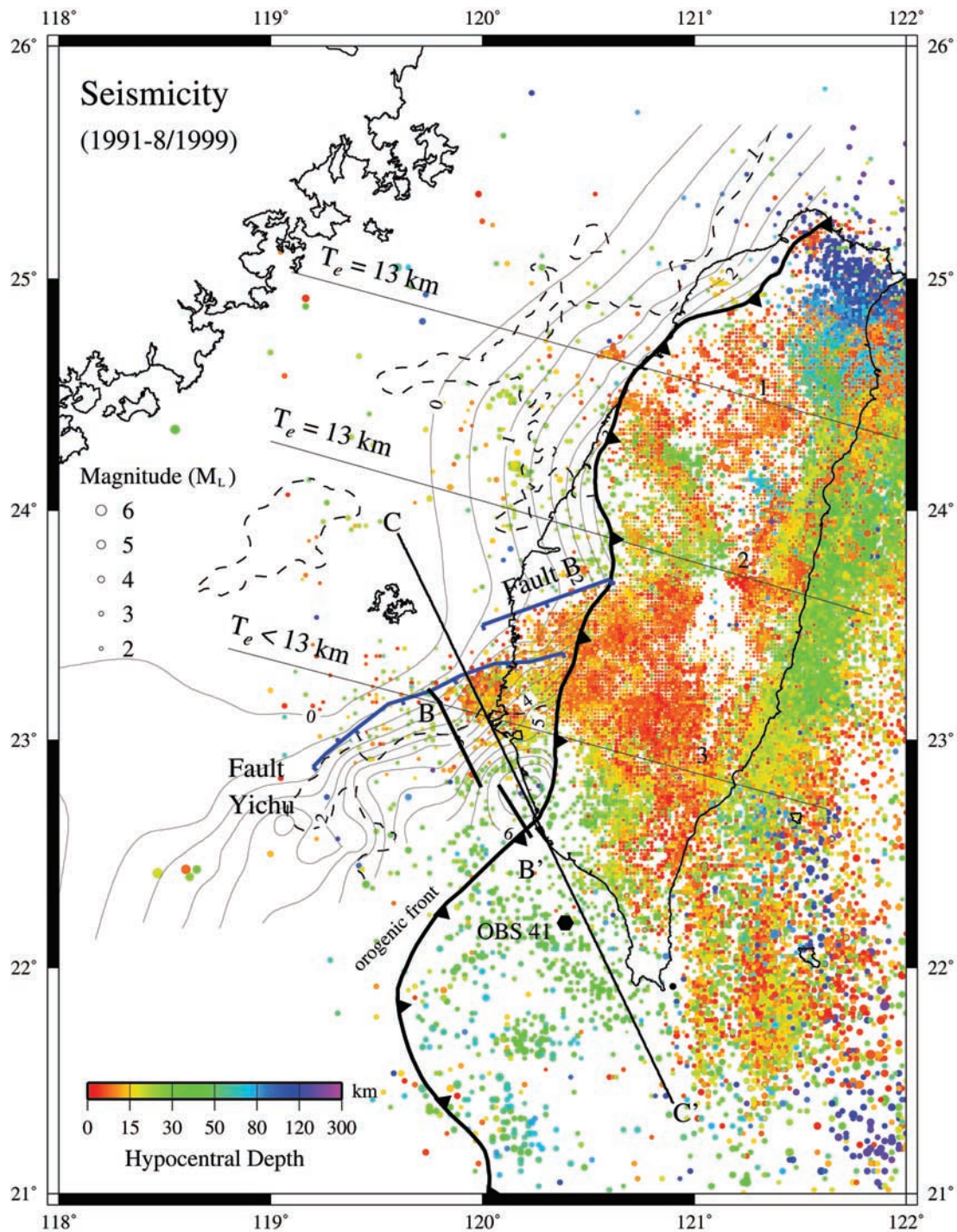
Figure 11. Seismicity of the West Taiwan basin and flanking regions based on historical data (January 1991 to August 1999) recorded by the Central Weather Bureau Seismic Network. The basin, west of the thrust front (barbed line), is generally associated with a low level of seismicity. The main exception is in the south where the base of the foreland basin sequence (gray contour lines) reaches its greatest curvature. Here there is abundant shallow seismicity that appears to align itself along the trend of Fault Yichu and Fault B and the local strike of the foreland flexure. The velocity structure beneath ocean bottom seismograph (OBS) 41 [*Nakamura et al.*, 1998] has been projected onto profile CC′ and is shown in Figure 12.

foreland basin. One possibility is that there are preexisting lines of weakness in the lithosphere that underlies the southern part of the Taiwan basin that have helped to focus the stresses induced by flexural loading. Seismic reflection

profile BB′ (Figure 13), which parallels profile CC', suggest the peak bending stress and high level of seismicity correlate with a major border fault, the Yichu Fault. The fault is known to have been active during the development of the
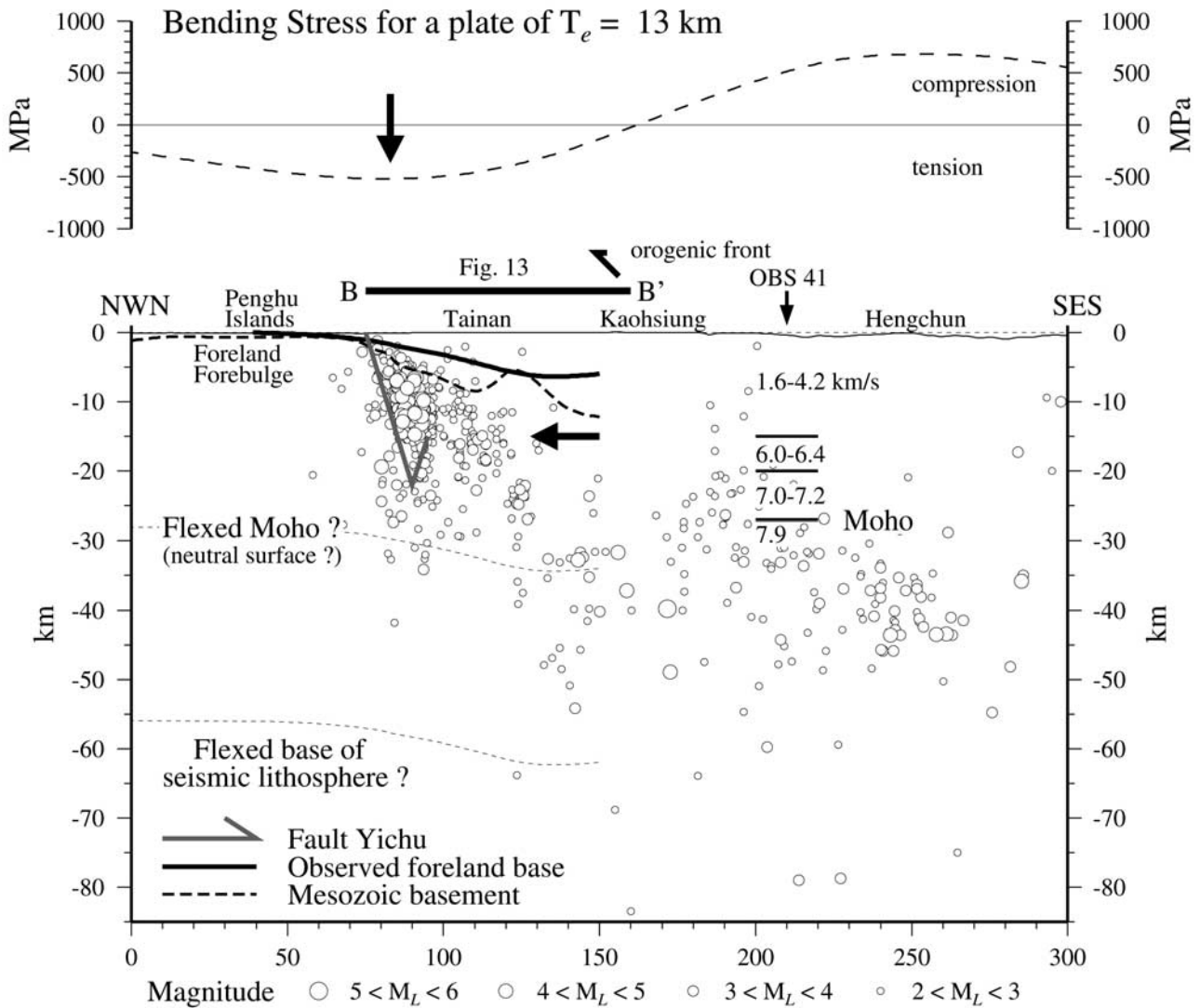
Figure 12. Flexure, bending stress, and seismicity along profile CC′ of the southern part of the West Taiwan basin. (top) Bending stress in the upper part of a flexed plate with $T_e = 13$ km, similar to the value deduced along profiles 1 and 2. (bottom) Historically active seismicity within a 10-km "window" either side of the profile. There is a close correlation between the peak in the tensile bending stress and a high level of seismic activity suggesting a link between them. The dashed lines show the hypothetical thickness of the short-term (? seismic) lithosphere. OBS 41 shows that the seismicity in the south part of the profile resides mostly in the crust and upper mantle. The location of seismic reflection profile BB′ (Figure 13) is shown as a heavy solid line.

underlying rifted margin [e.g., *Yang et al.*, 1991]. Furthermore, there is evidence of fault scarps on the seafloor (e.g., Figure 13), suggesting recent faulting. Therefore lithospheric flexure, in combination with the reactivation of underlying extensional faults, may have been a major control on seismicity patterns in the Taiwan region.

[52] Our calculations of foreland basin flexure and hence bending stress are based on models which assume that only vertical loads act on the lithosphere. They therefore do not take into account any horizontal stresses that act across the convergent plate boundary. *Hanks* [1971] argued, for example, from bathymetry and earthquake data seaward of the Kuril Trench that horizontal compressional stresses act across convergent plate boundaries which may be large enough to negate any extensional bending stress that might arise as a consequence of flexure. *Caldwell et al.* [1976], however, showed that large compressional stresses were not required to explain the seaward wall of all deep-sea trenches and that once individual profiles were normalized for their maximum depth and T_e, there was a certain "universality" to their shape.

[53] Although there is evidence for horizontal compression across the Taiwan orogenic belt [*Yeh et al.*, 1991], the stresses do not appear large enough to account for the seismicity in the West Taiwan foreland basin. We base this conclusion on two main observations. First, the style of faulting determined from focal mechanism studies of earthquakes beneath the West Taiwan basin is not dominated by thrust faults, as would be expected in a compressional setting. Rather, it is characterized by normal faulting [*Yeh et al.*, 1991; *Kao and Wu*, 1996], except in the region of
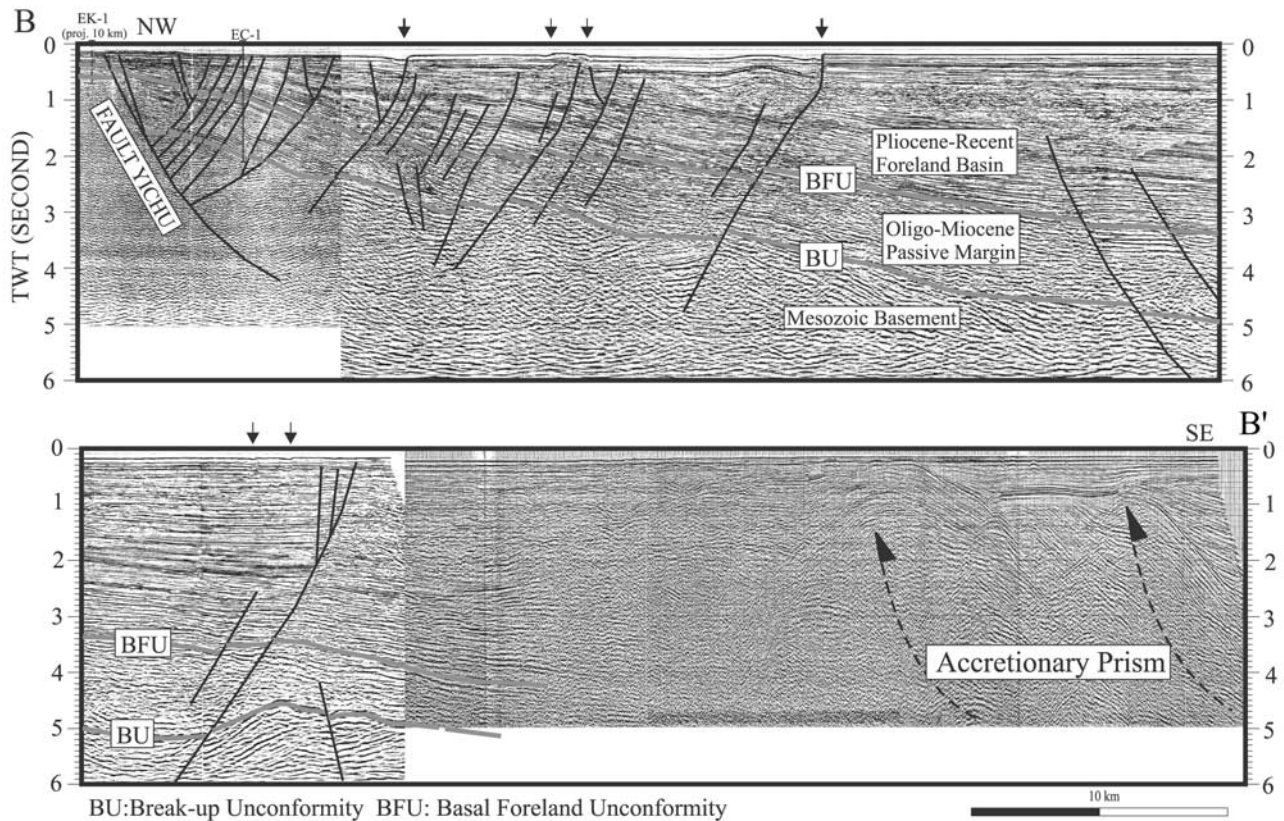
Figure 13. Seismic reflection profile BB′ of the southern part of the Taiwan basin, in the vicinity of profile CC′ (Figure 11). The profile shows a flexed and highly faulted base of the foreland sequence. The cluster of faults on the NW end of the profile correlates with a high level of relatively shallow (<25 km) seismicity. The presence of fault scarps on the seafloor (small vertical arrows) indicates recent faulting.

Fault Yichu, where normal faulting [*Yeh et al.*, 1991] occurs in addition to thrust [*Ma and Chen*, 1999] and strike-slip [*Rau et al.*, 1996] faulting. Second, seismic reflection profile data show that normal faulting (e.g., Figure 13) dominates the structural fabric of the foreland basin lithosphere, even for that part of the foreland that is immediately adjacent to the thrust front. Therefore, while regional horizontal compressional stresses may exist across the Taiwan region, they do not appear to be large enough either to negate extensional stresses being generated by lithospheric flexure or to prevent normal faulting from occurring in those regions of the flexed lithosphere that have failed rather than flexed.

6. Conclusions

[54] We draw the following conclusions from this study:

1. The West Taiwan basin formed by lithospheric flexure in front of migrating thrust and fold loads in the Taiwan orogenic belt. The basin developed ∼6.5 Ma on a rifted continental margin that underwent its last major rifting event ∼30−58 Ma.

2. Flexure modeling shows that the basin cannot be explained only by surface loading in the Taiwan orogenic belt and surrounding offshore regions. Other contributions are required. The most likely source is buried loading due to overthrusting of the lower crust on the upper crust, as indicated earlier by *Yeh et al.* [1998] from seismic refraction data.

3. Buried loading accounts for the presence of a prominent Bouguer anomaly high in east central Taiwan, a lateral offset of ∼20−30 km between the peak topography and the maximum depth of the seismic Moho and, an "upwarp" in the seismic interface between the lower and upper crust.

4. Profiles of the northern part of the basin can be explained by combined surface and buried loading and T_e = 13 km. These values are low when compared to some foreland basins but are similar to rift-type basins in passive continental margins. We attribute the low values to inheritance by the West Taiwan foreland of the thermal and mechanical properties of the underlying South China Sea continental margin.

5. The flexure models predict a bulge that extends from the continental shelf break, across the Taiwan Strait, intersecting the coast of China in the region of Fujian Province. The Penghu Islands are located a few kilometers to the east of the bulge crest, suggesting that orogenic loading is the cause of their tectonic uplift and, possibly, their high-level planation surfaces.

6. Profiles of the southern part of the basin cannot be explained as easily by elastic plate models. The high

curvature suggests that the southern part of the basin is yielding rather than flexing.

7. These differences in the flexural response along-strike of the West Taiwan basin are reflected in seismicity patterns west of the thrust front. The northern part of the basin is associated with a low level of seismic activity. In contrast, the southern part is characterized by an abundance of earthquakes, especially at shallow (<25 km) depths. The earthquakes cluster along two extensional faults that were active during rifting of the continental margin, suggesting that lithospheric flexure and the reactivation of preexisting faults are important contributors to the seismicity of the Taiwan region.

References

Abers, G. A., and H. Lyon-Caen, Regional gravity anomalies, depth of the foreland basin and isostatic compensation of the New Guinea Highlands, *Tectonics*, 9, 1479–1493, 1990.

Beaumont, C., Foreland basins, *Geophys. J. R. Astron. Soc.*, 65, 291–329, 1981.

Briais, A., P. Patriat, and P. Tapponnier, Updated interpretation of magnetic anomalies and sea-floor spreading stages in the South China Sea: Implications for the Tertiary tectonics of Southeast Asia, *J. Geophys. Res.*, 98, 6299–6328, 1993.

Burov, E. B., M. G. Kogan, H. Lyon-Caen, and P. Molnar, Gravity anomalies, the deep structure and dynamic processes beneath the Tien Shan, *Earth Planet. Sci. Lett.*, 96, 367–383, 1990.

Caldwell, J. G., W. F. Haxby, D. E. Karig, and D. L. Turcotte, On the applicability of a universal elastic trench profile, *Earth Planet. Sci. Lett.*, 31, 239–246, 1976.

Caporali, A., Gravity anomalies and the flexure of the lithosphere in the Karakoram, Pakistan, *J. Geophys. Res.*, 100, 15,075–15,085, 1995.

Chen, P.-Y., A review and discussion about the stratigraphic subdivision and some problems concerning the structural geology of the Peng-Hu islands, *Spec. Publ. Cent. Geol. Surv.*, 6, 9–38, 1992.

Chen, Y.-G., and T.-K. Liu, Sea level changes in the last several thousand years, Penghu islands, Taiwan Strait, *Quat. Res.*, 45, 254–262, 1996.

Chou, Y.-W., and H.-S. Yu, Structural expression of flexural extension in an arc-continent collisional foredeep of western Taiwan, in *Geology and Geophysics of an Arc-Continent Collision, Taiwan*, edited by T. B. Byrne and C.-S. Liu, *Spec. Pap. Geol. Soc. Am.*, 358, in press, 2002.

Desegaulx, P., H. Kooi, and S. Cloetingh, Consequences of foreland basin development on thinned continental lithosphere—Application to the Aquitaine Basin (SW France), *Earth Planet. Sci. Lett.*, 106, 116–132, 1991.

Haddad, D., and A. B. Watts, Subsidence history, gravity anomalies, and flexure of the northeast Australian margin in Papua New Guinea, *Tectonics*, 18, 827–842, 1999.

Hanks, T. C., The Kuril trench-Hokkaido system: Large shallow earthquakes and simple models of deformation, *Geophys. J. R. Astron. Soc.*, 23, 1971.

Heiskanen, W. A., and F. A. Vening-Meinesz, *The Earth and Its Gravity Field*, 470 pp., McGraw-Hill, New York, 1958.

Ho, C.-S., A synthesis of the geologic evolution of Taiwan, *Tectonophysics*, 125, 1–16, 1986.

Holt, W. E., and T. A. Stern, Subduction, platform subsidence, and foreland thrust loading: The late Tertiary development of the Taranaki Basin, New Zealand, *Tectonics*, 13, 1068–1092, 1994.

Hsu, S.-K., and J.-C. Sibuet, Is Taiwan the result of arc-continent or arc-arc collision?, *Earth Planet. Sci. Lett.*, 136, 315–324, 1995.

Hsu, S.-K., C.-S. Liu, C.-T. Shyu, S.-Y. Liu, J.-C. Sibuet, S. Lallemand, C.-S. Wang, and D. Reed, New gravity and magnetic anomaly maps in the Taiwan-Luzon region and their preliminary interpretation, *Terr. Atmos. Oceanic Sci.*, 9, 509–532, 1998.

Jordan, T. E., Thrust loads and basin evolution, Cretaceous, Western United States, *AAPG Bull.*, 65, 2506–2520, 1981.

Juang, W.-S., and J.-C. Chen, Geochronology and geochemistry of Penghu basalts, Taiwan Strait and their tectonic significance, *J. SE Asian Earth Sci.*, 7, 185–193, 1992.

Kao, H., and W.-P. Chen, The Chi-Chi earthquake sequence: Active out-of-sequence thrust faulting in Taiwan, *Science*, 288, 2346–2349, 2000.

Kao, H., and F. T. Wu, The 16 September earthquake (M_b = 6.5) in the Taiwan Strait and its tectonic implications, *Terr. Atmos. Oceanic Sci.*, 7, 13–29, 1996.

Kao, H., S. S. J. Shen, and K.-F. Ma, Transition from oblique subduction to collision: earthquakes in the southernmost Ryukyu arc-Taiwan region, *J. Geophys. Res.*, 103, 7211–7229, 1998.

Kao, H., G.-C. Huang, and C.-S. Liu, Transition from oblique subduction to collision in the northern Luzon arc-Taiwan region: Constraints from bathymetry and seismic observations, *J. Geophys. Res.*, 105, 3059–3079, 2000.

Karner, G. D., and A. B. Watts, Gravity anomalies and flexure of the lithosphere at mountain ranges, *J. Geophys. Res.*, 88, 10,449–10,477, 1983.

Keen, C. E., and S. A. Dehler, Extensional styles and gravity anomalies at rifted continental margins: Some North Atlantic examples, *Tectonics*, 16, 744–754, 1997.

Kruse, S., and M. K. McNutt, Compensation of Paleozoic orogens: A comparison of the Urals to the Appalachians, *Tectonophysics*, 154, 1–17, 1988.

Kruse, S., and L. H. Royden, Bending and unbending of an elastic lithosphere: the Cenozoic history of the Apennine and Dinaride foredeep basins, *Tectonics*, 13, 278–302, 1994.

Lin, A. T., Cenozoic stratigraphy and tectonic development of the west Taiwan basins, Ph.D. thesis, 246 pp., Univ. of Oxford, Oxford, UK, 2001.

Lin, C.-H., Y.-H. Yeh, H.-Y. Yen, K.-C. Chen, B.-S. Huang, S. W. Roecker, and J.-M. Chiu, Three-dimensional elastic wave velocity structure of the Hualien region of Taiwan: Evidence of active crustal exhumation, *Tectonics*, 17, 89–103, 1998.

Liu, C.-S., S.-Y. Liu, S. E. Lallemand, N. Lundberg, and D. Reed, Digital elevation model offshore Taiwan and its tectonic implications, *Terr. Atmos. Oceanic Sci.*, 9, 705–738, 1998.

Lyon-Caen, H., and P. Molnar, Constraints on the structure of the Himalaya from an analysis of gravity anomalies and a flexural model of the lithosphere, *J. Geophys. Res.*, 88, 8171–8191, 1983.

Lyon-Caen, H., and P. Molnar, Gravity anomalies and the structure of the western Tibet and the southern Tarim basin, *Geophys. Res. Lett.*, 11, 1251–1254, 1984.

Ma, K.-F., and J.-Y. Chen, Focal mechanism determinations of the 1991 Chiali earthquake (M_L = 5.7) sequence, *Terr. Atmos. Oceanic Sci.*, 10, 447–470, 1999.

Nakamura, Y., K. Mcintosh, and A. T. Chen, Preliminary results of a large offset seismic survey west of Hengchun Peninsula, southern Taiwan, *Terr. Atmos. Oceanic Sci.*, 9, 395–408, 1998.

Nissen, S. S., D. E. Hayes, P. Buhl, J. Diebold, B. Yao, W. Zeng, and Y. Chen, Deep penetration seismic soundings across the northern margin of the South China Sea, *J. Geophys. Res.*, 100, 22,407–22,433, 1995.

Pazzaglia, F. J., and T. W. Gardner, Late Cenozoic flexural deformation of the middle U. S. Atlantic passive margin, *J. Geophys. Res.*, 99, 12,143–12,157, 1994.

Price, R. A., Large-scale gravitational flow of supracrustal rocks, Southern Canadian Rockies, in *Gravity and Tectonics*, edited by K. A. De Jong and R. A. Scholten, pp. 491–502, John Wiley, New York, 1973.

Qureshy, M. N., Thickening of a basalt layer as a possible cause for the uplift of the Himalayas—A suggestion based on gravity data, *Tectonophysics*, 7, 137–157, 1969.

Rau, R.-J., and F. T. Wu, Tomographic imaging of lithospheric structures under Taiwan, *Earth Planet. Sci. Lett.*, 133, 517–532, 1995.

Rau, R.-J., F. T. Wu, and T.-C. Shin, Regional network focal mechanism determination using 3D velocity model and *sh/p* amplitude ratio, *Bull. Seismol. Soc. Am.*, 86, 1270–1283, 1996.

Royden, L. H., The tectonic expression slab pull at continental convergent boundaries, *Tectonics*, 12, 303–325, 1993.

Royden, L. H., and G. D. Karner, Flexure of the lithosphere beneath the Apennine and Carpathian foredeep: Evidence for an insufficient topographic load, *AAPG Bull.*, 68, 704–712, 1984.

Shiao, T.-W., and L. S. Teng, Flexural tectonics of western Taiwan foreland basin: A preliminary study, paper presented at the Third Taiwan Sysmpsium on Geophysics, Geophys. Soc. of China, Taipei, 1991.

Snyder, D. B., and M. Barazangi, Deep crustal structure and flexure of the Arabian plate beneath the Zagros collisional mountain belt as inferred from gravity observations, *Tectonics*, 5, 361–373, 1986.

Stewart, J., and A. B. Watts, Gravity anomalies and spatial variations of flexural rigidity at mountain ranges, *J. Geophys. Res.*, 102, 5327–5352, 1997.

Sung, Q., and Y. Wang, Sedimentary environments of the Miocene sediments in the Hengchun Peninsula and their tectonic implication, *Mem. Geol. Soc. China*, 7, 325–340, 1986.

Suppe, J., Mechanics of mountain-building and metamorphism in Taiwan, *Mem. Geol. Soc. China*, 4, 67–89, 1981.

Tanner, J. G., and R. J. Uffen, Gravity anomalies in the Gaspé Peninsula, *Publ. Dom. Obs.*, 21, 221–260, 1960.

Teng, L. S., Geotectonic evolution of late Cenozoic arc-continent collision in Taiwan, *Tectonophysics*, 183, 57–76, 1990.

Ting, H.-H., C.-Y. Huang, and L.-C. Wu, Paleoenvironments of the late Neogene sequences along the Nantzuhsien River, southern Taiwan, *Petrol. Geol. Taiwan*, 26, 121–149, 1991.

Walcott, R. I., Lithospheric flexure, analysis of gravity anomalies, and the propagation of seamount chains, in *The Geophysics of the Pacific Ocean Basin and Its Margin*, *Geophys. Monogr. Ser.*, vol. 19, edited by G. H. Scrutton, M. H. Manghnani, and R. Moberly, pp. 431–438, AGU, Washington, D. C., 1976.

Wang, C.-Y., and T.-C. Shin, Illustrating 100 years of Taiwan seismicity, *Terr. Atmos. Oceanic Sci.*, 9, 589–614, 1998.

Watts, A. B., Gravity anomalies, crustal structure and flexure of the lithosphere at the Baltimore Canyon Trough, *Earth Planet. Sci. Lett.*, 89, 221–238, 1988.

Watts, A. B., The effective elastic thickness of the lithosphere and the evolution of foreland basins, *Basin Res.*, 4, 169–178, 1992.

Watts, A. B., and M. Torné, Subsidence history, crustal structure and thermal evolution of the Valencia Trough: A young extensional basin in the western Mediterranean, *J. Geophys. Res.*, 97, 20,021–20,041, 1992.

Watts, A. B., S. H. Lamb, J. D. Fairhead, and J. F. Dewey, Lithospheric flexure and bending of the central Andes, *Earth Planet. Sci. Lett.*, 134, 9–21, 1995.

Wu, F. T., and R.-J. Rau, Seismotectonics and identification of potential seismic source zones in Taiwan, *Terr. Atmos. Oceanic Sci.*, 9, 739–754, 1998.

Yang, K.-M., H.-H. Ting, and J. Yuan, Structural styles and tectonic modes of Neogene extensional tectonics in southwestern Taiwan: Implication for hydrocarbon exploration, *Petrol. Geol. Taiwan*, 26, 1–31, 1991.

Yang, Y.-S., and T.-K. Wang, Crustal velocity variation of the western Philippine Sea plate from TAICRUST OBS/MCS line 23, *Terr. Atmos. Oceanic Sci.*, 9, 379–393, 1998.

Yeh, Y.-H., E. Barrier, C.-H. Lin, and J. Angelier, Stress tensor analysis in the Taiwan area from focal mechanisms of earthquakes, *Tectonophysics*, 200, 267–280, 1991.

Yeh, Y.-H., et al., Onshore/offshore wide-angle deep seismic profiling in Taiwan, *Terr. Atmos. Oceanic Sci.*, 9, 301–316, 1998.

Yeh, Y.-H., C.-H. Lin, B.-S. Huang, R.-C. Shih, and H.-Y. Yen, Variation of crustal thickness in Taiwan, inferred from wide-angle seismic data, *Eos Trans. AGU*, 80(46), Fall Meet. Suppl., F1042 1999.

Yen, H.-Y., Y.-H. Yeh, and C.-H. Chen, Gravity terrain corrections of Taiwan, *Terre. Atmos. Oceanic Sci.*, 5, 1–10, 1994.

Yu, H.-S., and Y.-W. Chou, Characteristics and development of the flexural forebulge and basal unconformity of Western Taiwan Foreland Basin, *Tectonophysics*, 333, 277–291, 2001.

Yu, N.-T., Sequence stratigraphy of the middle to upper Miocene strata, northern Taiwan: A preliminary study, *J. Geol. Soc. China*, 40, 685–707, 1997.

———————————

A. T. Lin, Department of Earth Sciences, National Central University, 300, Junga Road, Jungli, Taiwan. (andrew.lin@tpe.cpcoped.com.tw)

A. B. Watts, Department of Earth Sciences, University of Oxford, Parks Road, Oxford OX1 3PR, UK. (tony.watts@earth.ox.ac.uk)